Journal of Materials & Environmental Sustainability Research (2022), 2(1): 19-38
p-ISSN: 2811-1338; e-ISSN: 2811-132X
DOI: https://doi.org/10.55455/jmesr.2022.002

Original Research Paper

Biogenic silver-kaolinite nanocomposite for the sequestration of lead and cadmium in simulated produced water

Solomon E. Shaibu [1,2]*, Edu J. Inam [1,2], Eno A. Moses [1]

[1] Department of Chemistry, University of Uyo, Uyo, Nigeria
[2] International Centre for Energy and Environmental Sustainability Research (ICEESR), University of Uyo, Uyo, Nigeria
*Corresponding author: Shaibu E. Solomon (shaibusolomon@uniuyo.edu.ng)

Received: February 14, 2022; Revised: April 8, 2022; Accepted: April 10, 2022; Published: April 13, 2022

Handling Editor: Ime B. Obot

Abstract:
Biologically inspired nanocomposites are currently attracting significant recognition in view of their environmentally friendly, cost efficient and sustainable properties. In this study, silver-kaolinite nanocomposite (SKN) was synthesized using aqueous extracts from fresh leaves of *Aloe vera* as a bioreducing agent and employed for the removal of lead (Pb) and cadmium (Cd) ions from simulated produced water (SPW). Morphological properties of SKN were examined using transmission electron microscopy (TEM), scanning electron microscopy (SEM), x-ray diffraction (XRD), Fourier transform infrared spectroscopy (FTIR), energy dispersive x-ray (EDX) spectroscopy, Brauner-Emmett-Teller (BET) and ultraviolet-visible (UV-Vis) spectrophotometry with average particle size ranging from 45 to 60 nm. Different physicochemical parameters (initial concentration (10 - 120 mg/L), adsorbent dosage (0.01 - 0.2 g), pH (2 - 8) and contact time (5 - 150 min)) were investigated to ascertain the efficiency of SKN. The results revealed optimum adsorption of 142 and 120 mg/g for lead and cadmium ions respectively at initial metal concentration of 100 mg/L, 0.05 g of SKN dose and pH 6 for 60 min. Freundlich isotherm and pseudo-second order kinetic model adequately interpreted the equilibrium and kinetic data respectively.

Keywords: Silver-kaolinite nanocomposite (SKN); simulated produced water (SPW); kaolinite; *Aloe vera*; adsorption; heavy metals

DOI: 10.55455/jmesr.2022.002

1. Introduction

Globally, petroleum exploration, production and export of allied products are the mainstay of many economies but not without its attendant environmental challenges. One of such problems is the generation of produced water (PW) - water collected in subsurface formations discharged during oil exploitation and it contains dissolved organics, inorganics, naturally occurring radioactive materials (NORM) as well as microorganisms (Fakhru'l-Razi et al. 2009). PW also accounts for more than eighty percent of the wastes generated in the oil industry, and is the highest by product from oil and gas activities but its effective management despite current technology is challenging in terms of cost, efficiency and sustainability (Fakhru'l-Razi et al. 2009; Arthur et al. 2005; veil et al. 2004). The inorganic compounds in PW (predominantly trace metal ions) have been reported to be highly toxic and evasive in diverse media as a result of their geogenic nature, bioaccumulative properties, high mobility, bioavailability as well as their chemistry in aqueous media (Kouassi et al. 2019; Gao et al. 2018; Ondrasek et al. 2018; Barbieri et al. 2018; Hao et al. 2019).

Incidentally, the presence of significant levels of Pb and Cd in aqueous media from anthropogenic or natural sources adversely affects biological systems particularly in children even at levels considered hitherto low (How

and Yaacob 2015). Effects of lead and cadmium toxicity are apparent from manifestations of organ failures, nervous, reproductive damage and cancer cells proliferation (Assi et al. 2016; Trabelsi et al. 2016).

Advent of nanotechnology has opened frontiers of opportunity due to inherent unique properties of materials at the nanoscale particularly in the remediation of environmental media. Nanomaterials have enjoyed extensive applications in different spheres as a result of their diversity and chemistry which include but not limited to: water treatment (Teow et al. 2019; Vikrant and Kim 2019), metal ion reutilization (Deng et al. 2019) plant disease diagnosis and management (Khan et al. 2019) stem cell research (Aziz et al. 2019; Pacheco-Torgal 2019), construction (Dahlan et al. 2019), including catalysis (Zhu et al. 2019). It has been empirically proven that nanoparticles possess high surface area and potent reactivity though its wide applications are hampered by agglomeration and rapid oxidation tendencies (Phenrat et al. 2007; O'Carroll et al. 2013) which affect efficiency. Addressing the challenges of agglomeration and rapid oxidation in the synthesis of nanomaterials has necessitated the use of stabilizing agents (Lin et al. 2010) as support in the production of nanocomposites (Liu et al. 2014; Bhowmick et al. 2014; Yuan et al. 2009; Kim et al. 2013; Dorathi et al. 2012; Ghosh and Bhattacharyya 2002; Srinivasan et al. 2011) with reasonable success. Despite the aforementioned, scanty reports are available for the treatment of PW using green and sustainable nanocomposites.

Against this background, the kaolinite clay employed in this study has been reported to possess interesting properties from low cation exchange capacity compared to swelling clays, considerable surface area to available reactive sites on its surface which researchers have significantly explored (Ghosh and Bhattacharyya 2002; Srinivasan et al. 2011). According to Sarma et al. (2019), other classes of clay minerals have been more extensively studied than kaolinite in respect to its adsorption potential. Though the kaolin class ($Al_2Si_2O_5(OH)_4$ is a ubiquitous mineral that is unevenly distributed and like others in its group is considered highly stable, economical, recyclable and easy to handle (Li et al. 2019). In isolation, kaolinite might not be an excellent adsorbent but impregnation with nanoparticle enhances its inherent adsorptive, catalytic, mechanical and surface properties (Srinivasan et al. 2011).

Currently, researches are designed with ecological impact and sustainability plans in mind in a bid to ensure the process is as "green" as possible. In this direction, this study utilized *Aloe vera* leaf extracts as a replacement for sodium borohydride and other chemical reducing agents for the synthesis of SKN. Aloes belong to the family *Liliaceae orasphodelaceae* of genus plant with more than 150 species and mostly native to South Africa. The Aloe species primarily inhabit relatively dry and warm climates and can also live and reproduce for more than 20 years (Botes et al. 2008). *Aloe vera* like other of their related Aloe species contains more than 200 different bioactive constituents (Wintola and Afolayan 2011; Botes et al. 2008). Its anti-inflammatory, antioxidative, antimicrobial, anticancer and antipyretic properties are well recognized by researchers and trado-medical practitioners (Sánchez-Machado et al. 2017; Reynolds and Dweck 1999; Shin et al. 1997; Umano et al. 1999; Saccu et al. 2001; Adesuyi et al. 2012). The synthesis of nanoparticles via biological route is cleaner, biocompatible, cost effective and sustainable in agreement with Medda et al. (1995). However, the potency of the leaf extracts is more likely due to synergistic approach of multiple biological moieties rather than the action of an individual biomolecule (Botes et al. 2008) and these lend credence to reducing and capping properties of the plant (Narayanan and Sakthivel 2008).

The objective of this research is to biologically synthesize silver-kaolinite nanocomposite (SKN) by employing *Aloe vera* leaf extract as a reducing agent and also evaluate the efficiency of the SKN for the removal of lead and cadmium ions from SPW. Therefore, this research is targeted at enhancing the trace metal adsorptive properties of kaolinite with particular attention to environmental preservation (green) while also attenuating the contaminant load of PW. The effects of different parameters: initial metal concentration, solution pH, contact time, and SKN dosage on removal efficiency were investigated and data fitted onto several equilibrium and kinetic models. Importantly, the results of the study will provide adequate experimental data for possible scale-up in employing SKN for removal of trace metals from PW.

2. Materials and Methods

Analytical grade chemicals were used throughout the study as supplied without further purification and these include $AgNO_3$, $Pb(NO_3)_2$, $CdCl_2$ (Merck analysis grade), NaOH (Sigma Aldrich, Diegem, Belgium) and HCl

(Purity 37%, density 1.1 kg/cm^3, Riedel-deHaen, Buffalo, NY, USA) and kaolinite mineral. Deionised water was used for the preparation of all stock solutions.

2.1 Sample preparation and analysis

The SPW was prepared using analytical grade chemicals. Salts included $AlCl_3$, $CuCl_2$, $CdCl_2$, $PbCl_2$, CH_3CO_2K, KCl, $FeCl_3$, CH_3CO_2Na, Na_2CO_3, and NaCl while the organics were diesel fuel, ethanol, ethylene glycol, glycerol, hexane, 2-propanol, xylene and toluene. Solution pH was adjusted dropwise using NaOH or HCl. The pH and electrical conductivity of the SPW was determined with pH meter (pH Sensor InPro 2000i SG/120/9823) and EC meter (AD331 Professional Waterproof Conductivity-TEMP Portable Meter with GLP) respectively in line with Clay and Pichtel, 2019. Total metal concentrations were determined by Perkin Elmer AAnalyst 200 atomic absorption spectrophotometer as presented in Table 1.

Phytochemical analysis of the *Aloe vera* leaf extract according to standard operating procedures follows Benzidia et al. 2019 submission. The *Aloe vera* was identified by taxonomist and screened for the presence of phenol, saponin, alkaloids and flavonoids. Geologically, the sample location (Itu Local Government Area in Akwa Ibom State, Nigeria) represents a region marked by physical progression that characterized the progression of the Southern sedimentary Basin which lies between the Niger Delta and the Calabar Flank around the low-lying coastal/deltaic plains of Southern Nigeria (Obianwu et al. 2011).

Table 1: Composition of simulated produced water (SPW)

pH	EC (μS/cm)	Concentration (mg/L)							
		Na^+	K^+	Ca^{2+}	Cu^{2+}	Fe^{3+}	Cd^{2+}	Pb^{2+}	Al^{3+}
6.8	3400	12000	5000	2000	1000	500	100	100	300

EC = electrical conductivity

According to the procedure reported by Ma and Eggleton, (1999) for cation exchange capacity determination with a little modification, 0.2 g of the kaolinite and *Aloe vera* modified kaolinite were separately deposited onto a filter paper after washing for about 10 times with deionized water followed by replacement of exchangeable cations with 1 M barium chloride solution. Subsequently, it was dried at 60 °C, washed several times with copious amount of deionized water and the barium content in the kaolinite quantified using x-ray fluorescence technique to determine the CEC.

2.2 Synthesis of nanocomposites and kaolinite modification

In the synthesis of the SKN, firstly *Aloe vera* leaves and kaolinite were locally sourced. The *Aloe vera* leaves were thoroughly washed, dried at room temperature for 48 hours and finely cut into small pieces. The extract was prepared by boiling a 30 g of *Aloe vera* for 10 min and the resulting broth stored at 4 °C prior to utilization for synthesis similar to (Song and Kim 2009; Balachandar et al. 2019). On the other hand, the kaolinite was also carefully washed with deionized water, dried and pulverized into very fine pieces, soaked in 0.1 M HCl solution for 4 hours to remove extraneous and organic matter, washed again several times with deionized water and finally dried at 30 °C prior to SKN synthesis (Balachandar et al. 2019; Sharma et al. 2019). To a 5 g of pulverized kaolinite, 50 mL of *Aloe vera* extract was added, stirred for 3 hours, allowed to stand overnight and then dried to get *aloe vera* modified kaolinite before characterization.

Subsequently, a 5 g of the ground kaolinite sample was added to 10 mL solution of $AgNO_3$ to form slurry, stirred at 400 rpm for 3 hours and then a 50 mL of the *Aloe vera* broth was added to the slurry with constant stirring at 400 rpm for 12 hours before it was centrifuged, dried at 30 °C and finally crushed to fine powder according to synthesis (Balachandar et al. 2019; Sharma et al. 2019).

2.3 Characterisation

Beckman Coulter DU 730 Uv-vis spectrophotometer was used to record the surface plasmon resonance (SPR) of raw kaolinite, *Aloe vera* modified kaolinite and SKN in a wavelength range of 300 to 650 nm while surface

morphology was captured under a FEITM scanning electron microscope (Nova Nano SEM 230, FEI, Hillsboro, OR, USA). Functional group analyses of the samples were recorded over the range 4000 – 400 cm^{-1} using Shimadzu FTIR-8400S. Similarly, the method of X-ray diffraction (XRD) was used to investigate the material structure of clay, *Aloe vera* modified kaolinite and SKN. The XRD analysis was conducted with a Rigaku Miniflex 600 diffractometer (Cu-K, 40 kV, 40 mA, λ = 1.5406 Å). It used copper Kα radiation and a graphite monochromator to produce X-rays with a wavelength of 1.5406 Å. The samples were individually placed in a glass holder and scanned from 10° to 75°. This scan range covered all major species of kaolinite and SKN. The scanning rate was set at 10 min at 250C. The porosity and specific surface area were recorded on a BET surface area analyzer (Model Nova 2000e, USA).

2.4 Batch adsorption studies

Batch adsorption experiment for the removal of lead and cadmium ions from the SPW onto SKN was performed at temperature of 27 ± 2 °C. To a 100 mL solution of 10 – 120 mg/L of the SPW solution in different Pyrex conical flasks, (0.01 – 0.2) g of SKN was added and rigorously agitated on a thermostat shaker at 250 rpm for a contact time of (5 – 150) min at pH range of 2 to 8 and consequently centrifuged prior to AAS (atomic absorption spectroscopy) analysis (Sharma et al. 2019). The concentrations of the residual metal ions in the supernatant were accordingly read using AAS while amount or quantity adsorbed (Qe) was calculated by the expression in Equation 1. Importantly, accuracy of the adsorption experiments was guaranteed by triplicate runs of the tests and mean of the results reported.

$$Q_e = \frac{(C_O - C_e)}{w} \times V \qquad (1)$$

where C_o and C_e are the initial and equilibrium concentrations (mg/L), V is the volume of the metal solution (L) and w is the weight of the SKN (g).

2.5 Adsorption data analysis: Isotherm and kinetic models

Isotherm models are important tools for understanding the relationship between quantity of adsorbate adsorbed in respect to the concentration of adsorbate at constant temperature in order to understand the underlying mechanism of the process and this relationship is represented graphically (Özsin et al. 2019; Salman et al. 2011). Numerous mathematical expressions (models) employ experimental parameters to extrapolate and predict reaction conditions, type and nature of adsorption as well as energy requirement of the system. Many models widely used to explicate two parameter systems are Langmuir, Freundlich, Temkin, Dubinin-Radushkevich, Flory-Huggins and Hill isotherm (Foo and Hameed 2010; Vijayaraghavan et al. 2006).

Langmuir isotherm, a popular model represented by the linearized expression in Equation 2 assumes monolayer adsorption on a homogenous surface (Vijayaraghavan et al. 2006), while Freundlich isotherm (Equation 3) on the other hand describes a heterogeneous system with uneven surface where adsorbate can form multiple layers on the surface of the adsorbent but is limited to low concentration of the adsorbate (Foo and Hameed 2010). Similarly, Temkin model (Equation 4) takes cognizance of interaction between adsorbent and adsorbate and majorly apt for predicting gas phase equilibrium but inadequate in other systems (Foo and Hameed 2010). In this study, Langmuir, Freundlich and Temkin isotherms models were used to interpret the adsorption data by means of the appropriate equations.

$$\frac{C_e}{Q_e} = \frac{1}{Q_O K_L} + \frac{1}{Q_0} C_e \qquad (2)$$

$$R_L = \frac{1}{1 + K_L C_O} \qquad (2a)$$

$$\log Q_e = \log K_f + \frac{1}{n} log C_e \qquad (3)$$

$$Q_e = \frac{RT}{b_T} lnA_r + \frac{RT}{b_T} lnC_e \quad (4)$$

where C_e is the equilibrium concentration of the adsorbate (mg/L), C_o, Q_e and Q_o are the initial adsorbate concentration, amount of adsorbate adsorbed per unit mass of adsorbate (mg/g) and adsorption capacity respectively while (K_L) is the Langmuir equilibrium adsorption constant. The dimensionless R_L parameter indicates the degree of favourability of the Langmuir isotherm curve: its unfavourable if (R_L> 1), linear (R_L= 1), favourable (0 <R_L< 1) or irreversible (R_L= 0) (Özsin *et al.* 2019). The Freundlich constants k_F and n are indications of how favourable the adsorption process is and k_F is the adsorption capacity of the adsorbent. Deductions from Temkin isotherm equilibrium binding constant A_r, isotherm constant b_T, universal gas constant R (8.314 J/mol/K) and T absolute temperature (298 K) also give vital insights into the adsorption mechanism.

Adsorption kinetics show the rate of the adsorption capacity through time and it is a tool for identification of the types of adsorption mechanism in a given system. Some of the models used in this study to describe the adsorption kinetics behaviour are pseudo first order (Equation 5), pseudo second order (eq. 6) and Elovich models (Equation 7).

$$\log(Q_e - Q_t) = \log Q_{e,cal} - \frac{k_1}{2.303} t \quad (5)$$

$$\frac{t}{Q_t} = \frac{1}{k_2 Q_{e,cal}^2} + \frac{1}{Q_{e,cal}} t \quad (6)$$

$$Qt = \frac{1}{\beta} \ln \frac{\alpha_E}{\beta} + \frac{1}{\beta} lnt \quad (7)$$

The Q_e and Q_t are the amounts of adsorbates adsorbed (mgg^{-1}) at equilibrium and time t, while k_1, k_2, α and β are the pseudo first-order rate, pseudo second-order rate, initial adsorption rate and the desorption constants respectively.

3. Results and Discussion

3.1 Characterization

Transmission electron microscopy (TEM) images of SKN in Figures 1a, 1b and 1c and particle size distribution in Figure 1d show a high distribution of the majorly spherical silver nanoparticles on the kaolinite support as depicted by the micrographs with sizes below 100 nm. Related to the findings of Rauwel et al. (2015), the shape, size and dispersion rate of the silver nanoparticles on the kaolinite in Figure1a are highly influenced by nature of *Aloe vera* extract and experimental conditions while further attributing the high level of dispersion observed to capping properties of the plant extracts. The foregoing is similar and responsible for the observations in Figure 1a - c. In contrast to deductions of Phanjom et al. (2012) there were no pairing tendencies or assemblage of the particles in Figure 1a and b primarily as a result of coating potentials of the phytochemicals, thereby enhancing their surface area. However, unlike Phanjom et al. (2012) flavonoids and particularly phenols were established to inhibit clustering as a result of exceptional reducing and enveloping properties and this submission was also supported by Nadagouda and Varma (2008).

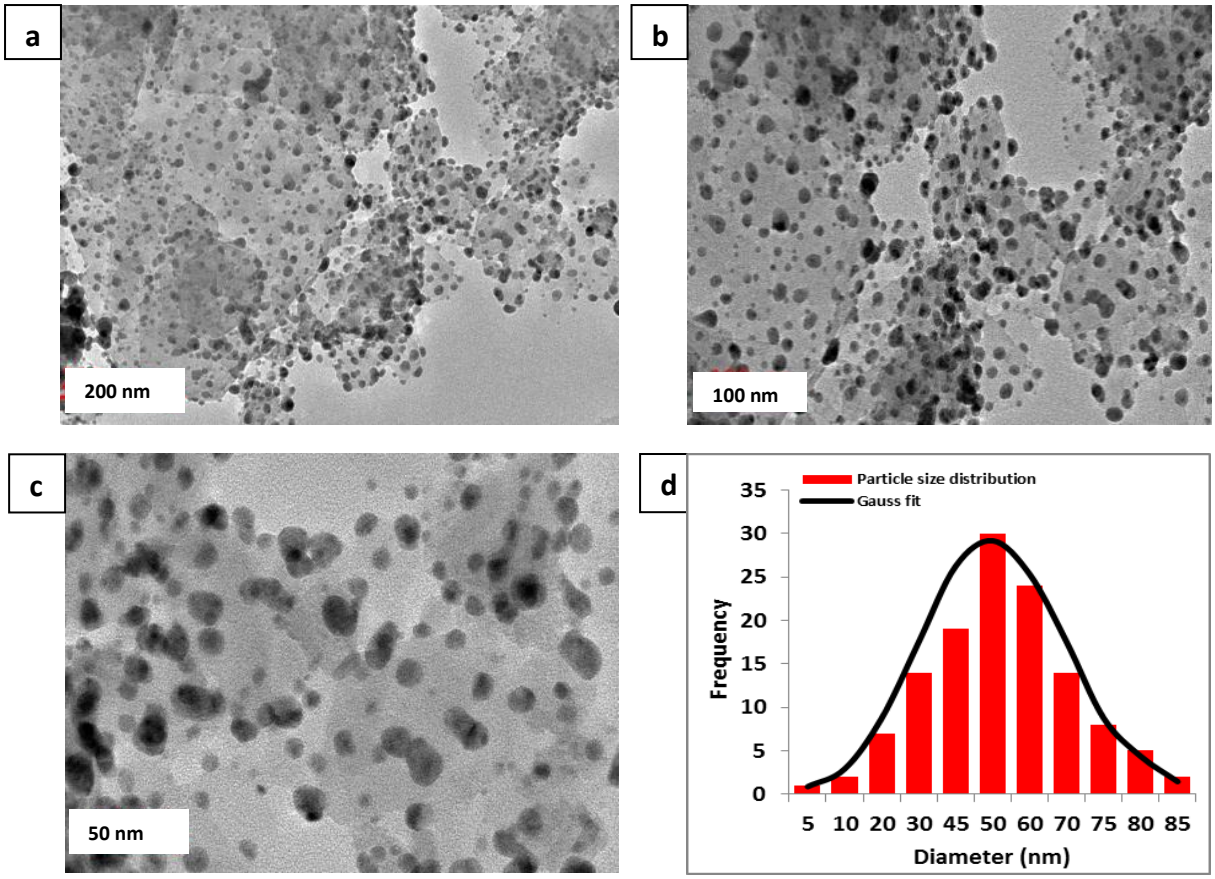

Fig. 1: TEM of (a). SKN at 200 nm (b) at 100 nm, (c) at 50 nm and (d) denotes particle size distribution for the biosynthesized SKN

Essentially, morphological characterisations of kaolinite, *Aloe vera* modified kaolinite and SKN carried out by scanning electron microscopy are shown in Figures. 2a - 2c. Particles in SKN (Fig. 1c) had more crevices and were stacked on one another mainly due to the bioactive constituents in the leaf extract as shown in Table 2 which contains saponin, phenol, alkaloid and flavonoids. This observation is supported by Medda et al. (2015), who posited that *Aloe vera* contains more than seventy active components. Significant agglomeration was observed with kaolinite sample (Fig. 2a) than others while *Aloe vera* modified kaolinite (Fig. 2b) and SKN (Fig. 2c) had evidence of discrete particles displaying lower level of aggregation owing to the capping effect of the biomolecules in the *Aloe vera* extract (Henglein 1998). The micrograph of SKN in 2c showed particles with irregular shapes and average sizes between 45 – 60 nm as corroborated by the size distribution in Figure 1d in addition to the presence of visible crevices and holes.

The energy dispersive x-ray spectra indicated the presence of silver alongside other elements that exist in the precursors used for the preparation of SKN. The elemental composition of the three materials (raw kaolinite, *Aloe vera* modified kaolinite and SKN) in Figures 2d, 2e and 2f consistently reflected the occurrence of significant levels (wt %) of oxygen (O), silicon (Si), aluminium (Al) and iron (Fe) which are naturally abundant in the kaolinite. The level of oxygen was comparatively higher in *Aloe vera* modified kaolinite and SKN than the raw kaolinite due to the oxygen bearing organic groups in the *Aloe vera* extract. Sarkar et al. (2019) reported a consonant outcome in their study.

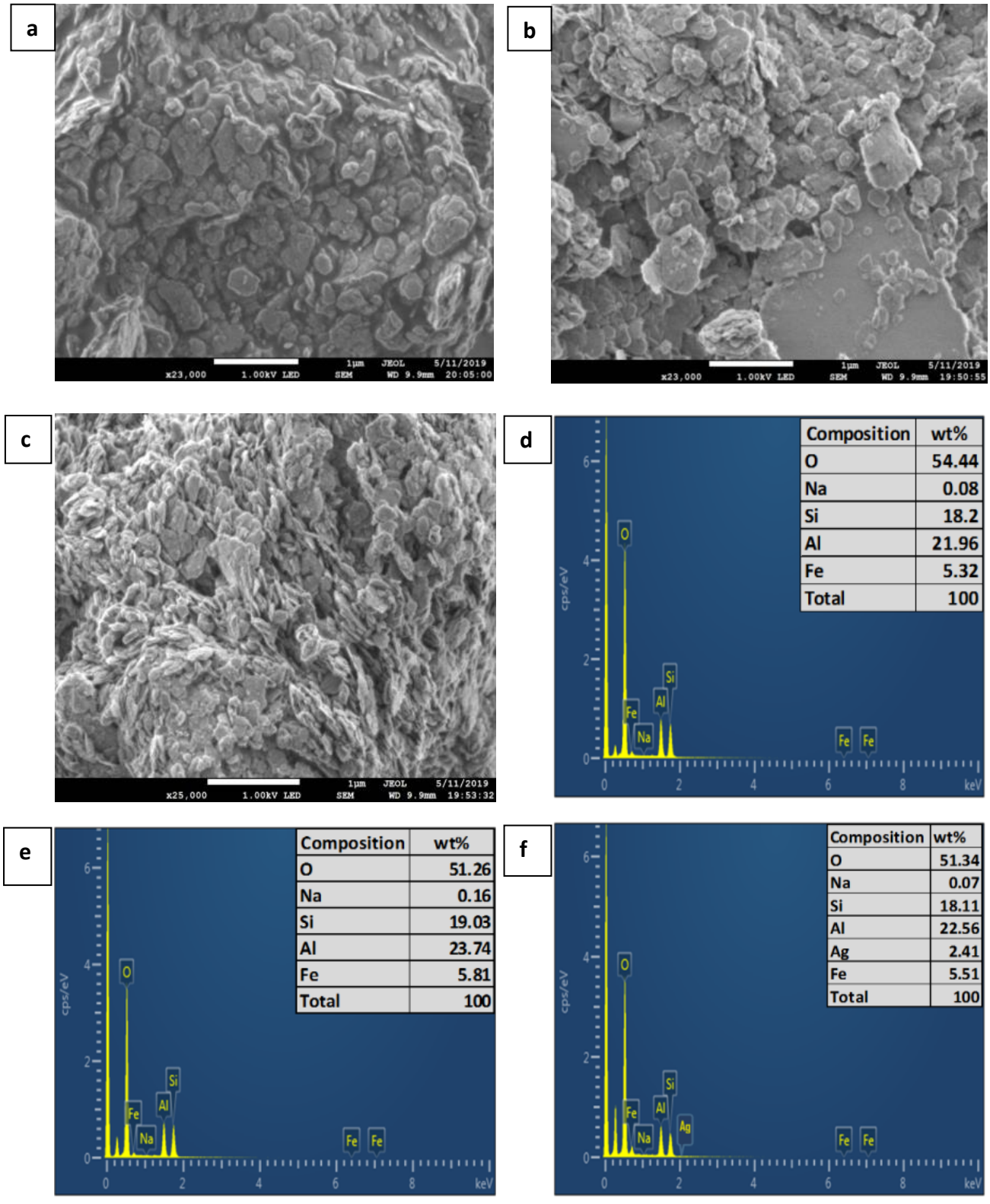

Fig. 2: SEM images of (a) kaolinite, (b) *Aloe vera* + kaolinite, (c) SKN and EDX of (d) kaolinite, (e) *Aloe vera* and (f) SKN

Surface area (SA) and pore sizes are two very important parameters that affect the chemical activity of a material and these features significantly distinguish nanomaterials from other porous engineered compounds. Catalytic activity, adsorption efficiency, biological potency and other applications of nanoparticles are basically hinged on the surface area of that material (Song and Kim 2009). Table 3 shows the surface area and pore sizes of kaolinite, kaolinite modified with *Aloe vera* and SKN while Figure 3a is the nitrogen adsorption-desorption isotherm of raw kaolinite, *Aloe vera* modified kaolinite and SKN. Observably, the BET specific surface area of SKN is higher than those of kaolinite modified with *Aloe vera* and which informs the choice of SKN as the adsorbent for the removal of these trace metals from SPW and a good candidate for water treatment. A submission supported by Sharma et al. (2019). The mesoporous nature of the SKN informed by pore size of 11.952 nm as shown in Table 3 is higher than the radius of Pb^{2+} (~ 0.12 nm) and Cd^{2+} (0.158 nm), these differential in pore size prominently facilitates the inward movement of ions into the SKN pores as similarly observed by Wang and Luo (2020). Noteworthy is the distribution of the pore volume in the order SKN>*Aloe vera* modified kaolinite>kaolinite which is primarily due to the treatment of kaolinite with the extract and the impregnation of kaolinite with silver to form SKN. As observed in many studies (Veil et al. 2004), (Koyuncu et al. 2007) and (Panda et al. 2010), modification of kaolinite clay minerals often leads to changes in surface and pore properties but often highly dependent on the amendment agent (temperature, pH, acid, plant extracts, etc.). Notwithstanding the submission of Sarma et al. (2019), some modification agents are quite caustic and tend to alter or destroy the crystalline structure of the kaolinite (Torres-Luna and Carriazo 2019; Gao et al. 2016) but *Aloe vera* extract on the other hand is confirmed to be eco-compatible thereby preserving the original phase configuration of the kaolinite while favourably enhancing the surface properties.

Over the years, Uv-vis spectroscopy has been embraced as fast, simple, accurate and economical method of analysis (Acevedo et al. 2007). This technique measures variations as a result of transitions in energy levels when radiation of the appropriate wavelength is absorbed (Kumar 2006). The production of SKN when *Aloe vera* extract was added became apparent with colour change to light brown similar to the reports of (Song and Kim (2009) and Roseline et al. 2008)) reports. The appearance of a strong absorption peak at about 410 nm in the spectrum of SKN that is absent in kaolinite and *Aloe vera* modified kaolinite spectra matches the SPR band of silver nanoparticles. According to information from Wani et al. (2011), Song and Kim (2009) as well as Shankar et al. (2004) it can be asserted in this case that silver was successful impregnated into the kaolinite matrix as shown Figure 3b.

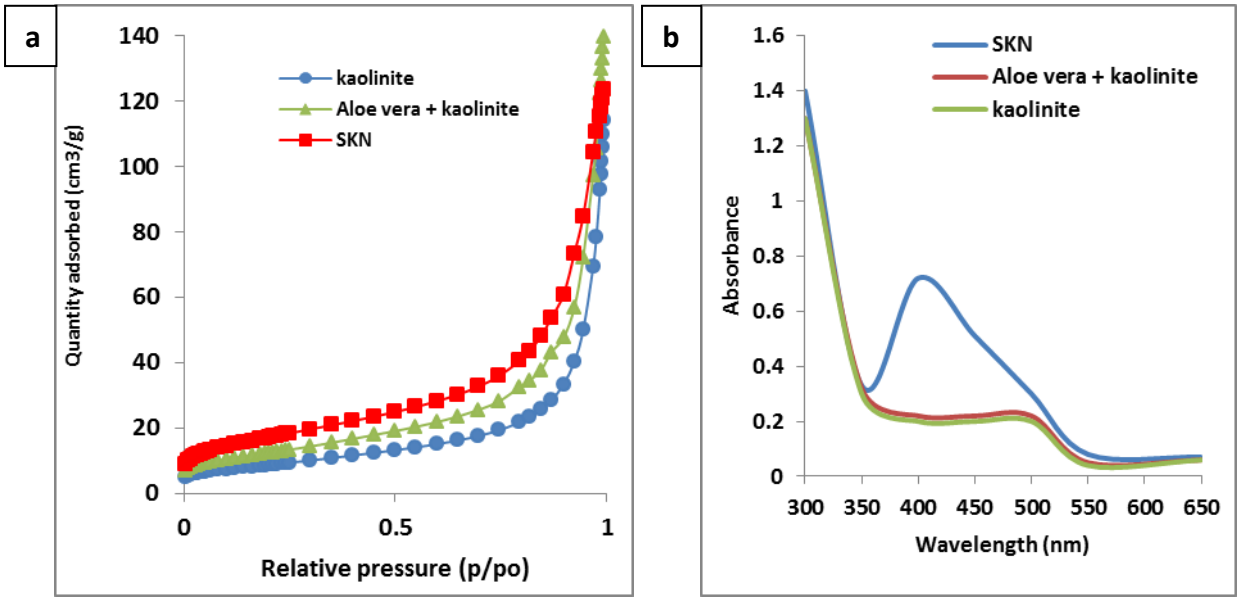

Fig. 3: Nitrogen adsorption-desorption isotherm of kaolinite, Aloe vera+ kaolinite, SKN and (b) Uv-visible spectra of kaolinite, Aloe vera + kaolinite and SKN

The crystallographic pattern of the kaolinite, *Aloe vera* modified kaolinite and silver-kaolinite nanocomposite (SKN) are presented in Figure 4 can be indexed to (001), (003), (004), (100), (111), (200) and (220) planes of kaolinite while d-value, intensity and broadness of peaks were observed after treatment with *Aloe vera* leaf extract. Prominent reflections corresponding to kaolinite and quartz can be observed in the XRD patterns of all the samples which is attributed to the use of the parent material (kaolinite). However, the intensities of the reflections are stronger in the kaolinite sample treated with *Aloe vera* indicative of higher degree of crystallinity than in the raw kaolinite and SKN in agreement with How and Yaacob (2015) and Wani et al. (2011). The diffractogram in Figure 4 revealed evident reflections of kaolinite (001), quartz (100,101), chlorite (004) and illite (003) in all the samples (kaolinite, *Aloe vera* modified kaolinite and SKN) as shown in Table 4 but smectite mineral was consistently absent in all the samples. These other phases (quartz, chlorite and illite) of clay minerals also influence the significant uptake of the Pb and Cd ions in the SPW as corroborated by Ouyang et al. (2019). The diffractogram was not affected by the eco-modification process using *Aloe vera* leaf extract due to the mild and noncorrosive nature of the metabolites present. Similarly, the reflections attributed to silver nanoparticles in the kaolinite matrix of the SKN were present without distortion of the base diffractogram. The pattern of SKN showed reflections characteristic of silver with face centered cubic (fcc) symmetry synonymous with silver and reflections indexed as (111), (200) and (220) at around 2θ of 38.21°, 44.01° and 64.13° respectively (Joint committee on powder diffraction standards file no:04-0783). Reflections at about 2θ of 12° represent kaolinite phase and sharp peaks around 21° and 26° ascribed to quartz were significantly present in the SKN pattern as well as all the samples. In addition, amorphosity of the nanomaterials is revealed by the broad nature of some reflections at 38° and 44° while the fundamental structural arrangement of the kaolinite was observed in *Aloe vera* modified clay and SKN buttressing the mild nature of the *Aloe vera* leaf extracts. Contrary to amorphism that is spotted when elevated temperature (Cheng et al. 2019) or concentrated solvents (Sarma et al. 2019) are employed, treatment of kaolinite with *Aloe vera* purified and increased the crystallinity of the phases present thereby improving adsorption efficiency.

The presence of active groups on the surface of SKN as a result of interaction with *Aloe vera* extract confers significant functionality on the SKN as corroborated by Tran et al., (2015) and evident in Figure 5. Absorption bands at 3700 cm^{-1}, 2820 cm^{-1} and 1618 cm^{-1} are ascribed to O-H stretching group of amide, CH_2 group bending vibration and C=O groups respectively while presence of Si-O bands at 1100 cm^{-1} to 900 cm^{-1} in all the spectra is atributed to the alumino silicate nature of the kaolinite. Sharp and less intense absorption bands around 3650 and 1620 cm^{-1} were duly ascribed to Al–Al–OH stretching band and bending modes of water molecules majorly due to the wet method of synthesis and the plant extract analogous to Liu and Lian (2019). The spectrum of SKN was intense and evident shifts to lower wavelengths primarily due to interaction between the biomolecules in the *Aloe vera* leaf extract, the kaolinite and silver nanoparticle was also observed. As posited by Sarkar et al., (2019) negatively charged functional groups present on the surface of SKN could increase the cations adsorption capacity.

Table 2: Qualitative phytochemical analysis of *Aloe vera* extract

Phytochemicals	Results
Phenol	+
Saponin	+
Alkaloid	+
Flavonoid	+

(+): present

Table 3: Surface area and pore size analysis of SKN, *Aloe vera* modified kaolinite and kaolinite

Materials	BET surface area (m^2/g)	Pore size (Å)	Pore vol (cm^3/g)
Kaolinite	31.1545	223.628	0.2069
Aloe vera modified kaolinite	44.6404	187.449	0.2192
SKN	61.8733	119.518	0.2549

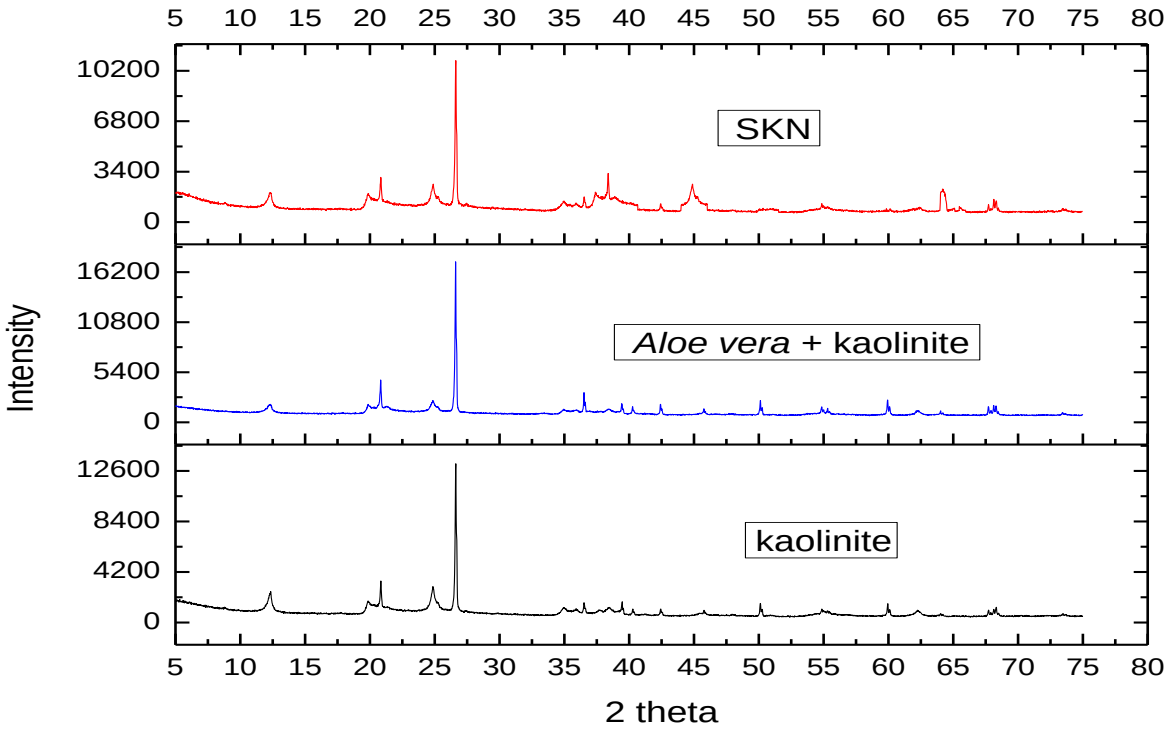

Fig. 4: XRD of kaolinite, *Aloe vera* + kaolinite and SKN

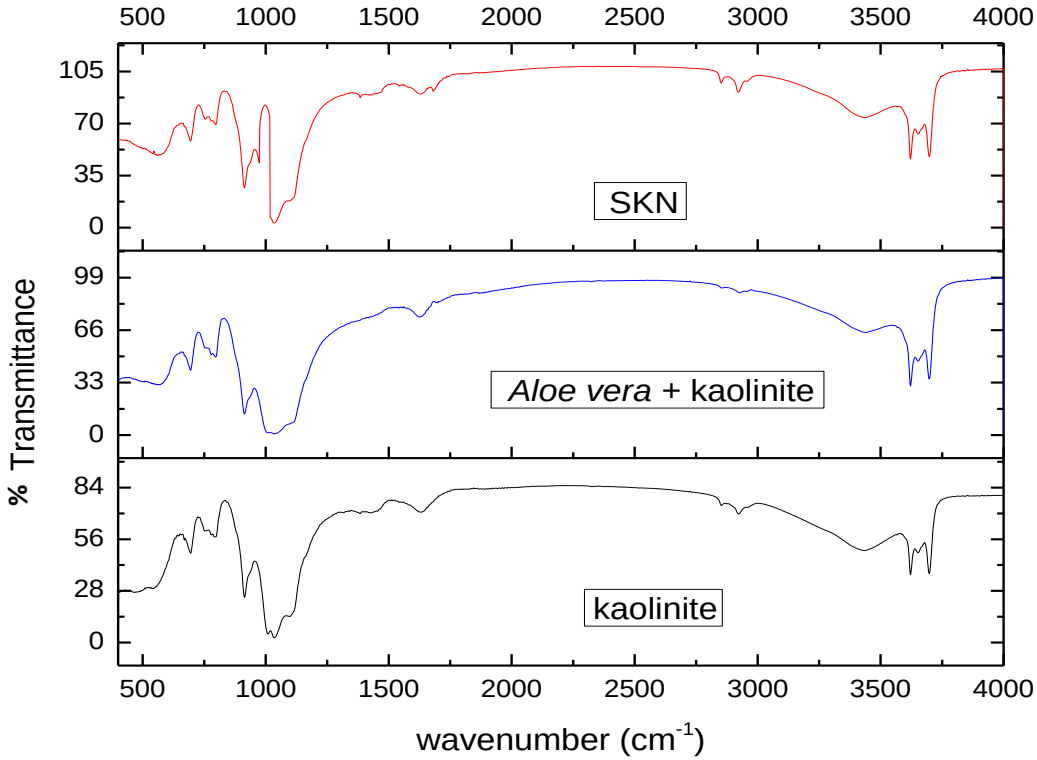

Fig. 5: FTIR spectra of kaolinite, kaolinite + *Aloe vera* and SKN

Table 4: XRD reflections of kaolinite, *Aloe vera* modified kaolinite and SKN

Kaolinite		*Aloe vera* + kaolinite		SKN		Mineral/planes
2θ°	d(Å)	2θ°	d(Å)	2θ°	d(Å)	
12.40	7.14	12.42	7.13	12.44	7.12	kaolinite (001)
21.00	4.23	20.94	4.24	21.02	4.23	quartz (100)
24.88	3.58	24.88	3.58	24.88	3.58	chlorite (004)
26.84	3.32	26.80	3.33	26.84	3.32	quartz (101), illite (003)
				38.21	2.35	silver (111)
				44.01	1.91	silver (200)
				64.13	1.39	silver (220)

The cation exchange capacity of the kaolinite and *Aloe vera* modified kaolinite were 3.881 and 5.125 Cmol/kg respectively which highly dependent on the mineralogical composition, formation processes, history, pH and amount of organic matter of the kaolinite as well as organic moieties in the *Aloe vera* leaf extract. The CEC value of kaolinite in this study was clearly higher than that of pure sand as reported by many authors (Battaglia et al. 2006; Ma and Eggleton 1999; Sadasivam and Rao 2016) but in close range to that reported by Errais et al., (2012). However, this value is comparatively lower than those reported for montmorillonite, halloysite and smectite (Ma and Eggleton 1999). They also attributed kaolinite's low CEC to isomorphous substitution within the kaolinite tetrahedral sheet or broken edges of OH planes accessibility. Incidentally, the influence of pH on kaolinite's CEC is well documented and opined to have a direct relationship. As such, repeated and thorough washing of the kaolinite with deionised water is believed to reduce the influence of pH on the CEC as the pH is brought to near neutrality. In addition, superficial basal charges according to Ma and Eggleton 1999 contributes to ion exchange interactions of kaolinite and Errais et al., (2012) submitted that in its unmodified state, there is preference for adsorption cations than anions due to the presence of negatively charged layers. These inherent properties affect the overall adsorption capabilities of SKN of Pb and Cd from SPW. Due to the possible modification by the abundant organic molecules with bulky functional groups in the *Aloe vera*, there was a little increase in the CEC which is similar to the observation of incorporating quaternary ammonium cations into clay mineral to prepare organoclay minerals as reported by Sarkar et al., (2019). This overall modification leading to higher CEC and impregnation with silver nanoparticles could be responsible for the high removal capacity of SKN.

3.2 Adsorption studies

Experimental parameters that highly influence a typical adsorption process of trace metals, dyes suspended or dissolved organics from aqueous media include initial concentration, adsorbent dosage, temperature, solution pH and contact time. The aforementioned factors affect the surface chemistry and interactions of the adsorbate and adsorbent.

3.3 Effect of initial metal concentration

Availability of binding sites and interaction of the metal ions with SKN surface determines the amount of adsorbate that will be trapped in the pores of the adsorbent. The results in Figure 6a showed that amount adsorbed increased slowly to 60 mg/L, plateaued to 80 mg/L before a sharp surge in adsorption to a peak of 142 and 120 mg/g for Pb and Cd ions respectively. Equilibrium was attained in 60 min at a concentration of 100 mg/L. Basically, the quantity adsorbed increased with increase in concentration till the available adsorption sites were saturated in addition to antagonistic or complementary ionic competition in SPW as similarly observed by Eren and Acar (2006). Both metal ions (Pb^{2+} and Cd^{2+}) showed analogous response patterns in the presence of SKN at the existing experimental conditions. Related to the report by Salman and Hameed (2011), it is adduced that higher adsorption sites at early stages and repulsive forces between the metal ions and SKN at equilibrium are reasons for the observed adsorption behaviour in Figure 6a.

3.4 Effect of SKN dosage

The optimum quantity of SKN required to sequestrate a particular concentration of metal ions is determined by varying the dose of the adsorbent until the optimum amount is ascertained. The purpose could be to establish the smallest effective quantity that could adsorb the metal ions both for economic reasons and efficiency (Salleh et al. 2011). As seen in Figure 6b, increase in SKN dose showed equivalent increase in the amount of metal ions adsorbed. The optimum dose was at 0.05 g while subsequent increase in the dosage did not significantly affect the quantity of metal ions adsorbed. This trend could be attributed to the availability of more surface area and active sites with adequate quantity of SKN. At 0.1 to 0.2 g of SKN, steric effect and electrostatic repulsion from the complex mixture of ions in the SPW started interfering with the process and precluded the incoming metal ions from attaching to the adsorption sites thereby plateauing at this point. Similarly, as observed in Figure 6b, the quantity of Pb^{2+} and Cd^{2+} adsorbed per unit mass plateaued between 0.1 and 0.2 g with increase of SKN. According to Shukla et al. (2002), high adsorbent concentration increases the collision between the particles and chances of particle agglomeration was high leading to a significant decrease in the total surface area and an increase in diffusional path length, both of which contribute to the decrease in the sorption capacity of metal ions on bentonite (Shukla et al. 2002). Analogous response was reported by Gupta and Bhattacharyya (2008).

3.5 Effect of solution pH

Another very vital factor that affects adsorption process is the pH of the solution, essentially modified by addition of 0.1 M HCl or NaOH as the case may be to the desired value. The alteration of the pH from acidic to basic imparts the solution chemistry, solubility of metal ions and SKN's surface response (Hu et al. 2006; Özsin et al. 2019). As shown in Figure 6c, the quantity adsorbed increased sharply when pH increased from 2 to 4 for both metals but the highest adsorption capacity was noticed at pH 6. Influence of pH was limited to a range of pH 2 to 8 due to precipitation of the metals above the range chosen (Wang et al. 2020), Adsorption was principally not favourable at lower pH due to competition between the hydrogen/hydroxonium ions (H^+/H_3O^+) and Pb^{2+} and Cd^{2+} for the available binding sites on the surface of SKN and further attributed to higher abundance of (H^+/H_3O^+) in comparison to the available metal ions (Pb^{2+} and Cd^{2+}) as opined by Gupta and Bhattacharyya (2008). The solution chemistry at higher pH values facilitated the depletion of (H^+/H_3O^+) while Pb^{2+} and Cd^{2+} preferentially bind to the SKN surface via an exchange mechanism and this observation is supported by several studies conducted by Gupta and Bhattacharyya (2008), Kumric´ et al. (2013), Jiang et al. (2010), and Bourliva et al. (2013).

3.6 Effect of contact time

This parameter is a very critical indicator of efficiency, economic feasibility and simplicity in the design of large-scale system (de Freitas et al. 2019). And in this study, the residence time for SKN was about 60 min making it a competitively favourable adsorbent. In addition, adsorption of Pb^{2+} and Cd^{2+} was noticeably fast at the beginning of the process between 5 and 40 min until 60 min into the agitation when the available active sites were saturated after which no significant change in the quantity adsorbed by SKN was observed. Aside from availability of active sites, possible interaction with surface active substituents of SKN contributes to the rapid uptake of the Pb^{2+} and Cd^{2+} at initial adsorption stage which is in concord with Wang and Luo (2020). Though there was no glaring increase in the quantity adsorbed after 60 min, "fast removal" phenomenon was apparent due to attainment of equilibrium within the first 60 min as hypothesized by Freitas et al. (Freitas et al. 2018b). Subsequently, after 60 min of constant agitation of Pb^{2+} and Cd^{2+}in the presence of SKN, inaccessibility of the residual unoccupied surface sites accounted for the evident plateauing of the adsorption as seen in Figure 6d. In addition, Bourliva et al. (2013) submitted in line with observation in this study that the difficulty observed at the latter stage of the adsorption process shown in Figure 6d significantly emphasizes interplay of resistance between the adsorbates in SPW with the SKN surface between 60 and 150 min.

Graphical representation of the interaction between the adsorbate and the SKN at constant temperature gives insight into a critical segment of the adsorption process (Özsin et al. 2019; Salman et al. 2011). Freundlich isotherm (Fig. 7a) adequately interpreted the adsorption behaviour of Pb^{2+} and Cd^{2+} onto SKN as reflected by the near unity correlation coefficient (0.9977 and 0.9901) as shown in Table 5. More so, the values of n (0.44263 and 0.5557) for Pb^{2+} and Cd^{2+} respectively highlight the intensity of the adsorption. Deductions from the Freundlich isotherm also posits that the surface of the SKN is heterogeneous as can be observed from the SEM in Figure 2a and both

Pb^{2+} and Cd^{2+} form multilayers on the SKN surface during its removal supported by (Özsin et al. 2019). The RL values (0.9588 and 09727) of Pb^{2+} and Cd^{2+} in Table 5 which are derivative of Langmuir isotherm (Fig. 7b) are individually less than 1 thereby buttressing the favourability of the adsorption process for both metal ions onto SKN while calculated Qo (208.33 and 185.185) was not quite close to the experimental values of 140 and 120 mg/g as corroborated by the low R^2 value. Temkin isotherm (Fig. 7c) on the other hand did not adequately interpret the equilibrium data going by the low correlation coefficients of 0.7876 and 0.8767 for Pb^{2+} andCd^{2+} respectively.

Basically, as reported by many authors that adsorption kinetics involve three steps which include diffusion of ions between the liquid phase and liquid-solid interface, movement from liquid–solid interface to solid surfaces and dispersion of ions into pores and crevices (Uğurlu and Karaoğlu 2011; Liao et al. 2013; Sheela et al. 2012; Alshameri et al. 2018). Pseudo-second order kinetic model with correlation coefficients of 0.9998 and 0.9873 in Figure 8b adequately interprets the kinetic data for Pb^{2+} and Cd^{2+} adsorption respectively. Importantly, the calculated quantity adsorbed (Qe, cal) for both metals (133.33 and 120.8) mg/g were in good agreement with the experimental values of 142 and 120 mg/g. The aforementioned deduction is validated by the assertion of Salman and Hameed (2011), where the rate of adsorption is opined to be highly dependent on availability of adsorption sites than initial concentrations (Salman and Hameed 2011). In addition, the closeness of R^2 to unity and significant disparity between the calculated quantity adsorbed (Qe, cal) of 53.133 and 55.188 mg/g in Table 6 and the experimental values (142 and 120) mg/g show that pseudo-first order is a poor fit of the data and by extension, the Elovich model as well.

In comparison with other studies as shown in Table 7, SKN has a significantly higher quantity adsorbed value than many of the adsorbents except that of Sheela et al. (2012) which could be as a result of the less competitive aqueous system in which the study was conducted.

4. Conclusion

This study revealed that silver-kaolinite nanocomposite (SKN) synthesized via bioreduction with *Aloe vera* leaf extract can be effectively used to remove lead (Pb) and cadmium (Cd) ions from SPW. The biological route of synthesis employed is cleaner, eco-compatible and consolidates the potential of using SKN for the treatment of PW. Notably, adsorption efficiency of SKN is highly influenced by the initial metal concentration, solution pH, adsorbent dosage and contact time. The SKN can be used as a substitute or synergistically with existing conventional treatment processes. Rate of adsorption was also dependent on availability of adsorption sites as ascertained by pseudo-second-order kinetic model which adequately interpreted the kinetic data while Freundlich isotherm model comparatively gave a better description of the entire adsorption process.

Table 5: Adsorption isotherm parameters and correlation coefficient of Pb^{2+} and Cd^{2+}

Isotherm models	Parameters	Values	
		Pb	Cd
Freundlich	K_F (mg/g(mg/L)^n)	0.0252	0.1259
	n	0.4263	0.5557
	R^2	0.9977	0.9901
Langmuir	Q_o (mg/g)	208.333	185.185
	K_L(L/mg)	0.043	0.028
	R_L	0.9588	0.9727
	R^2	0.7035	0.5768
Temkin	A_r(L/g)	1.02	8.494
	b_T(J/mol)	3.3×10^6	2.1×10^6
	R^2	0.7876	0.8767

Table 6: Kinetic parameters for the adsorption of Pb^{2+} and Cd^{2+} onto SKN

Kinetic models	Parameters	Values	
		Pb	Cd
Pseudo-first order	K_1 (min^{-1})	0.01382	0.02418
	$Q_{e,cal}$(mg/g)	53.113	55.808
	R^2	0.6607	0.7347
Pseudo-second order	K_2 ($g.mg^{-1}.min^{-1}$)	0.00105	0.00132
	$Q_{e,cal}$(mg/g)	133.33	120.48
	R^2	0.9998	0.9873
Elovich	α_E ($g.min^2/mg$)	0.0587	0.05312
	β (g.min/mg)	10.957	7.840
	R^2	0.7549	0.8093

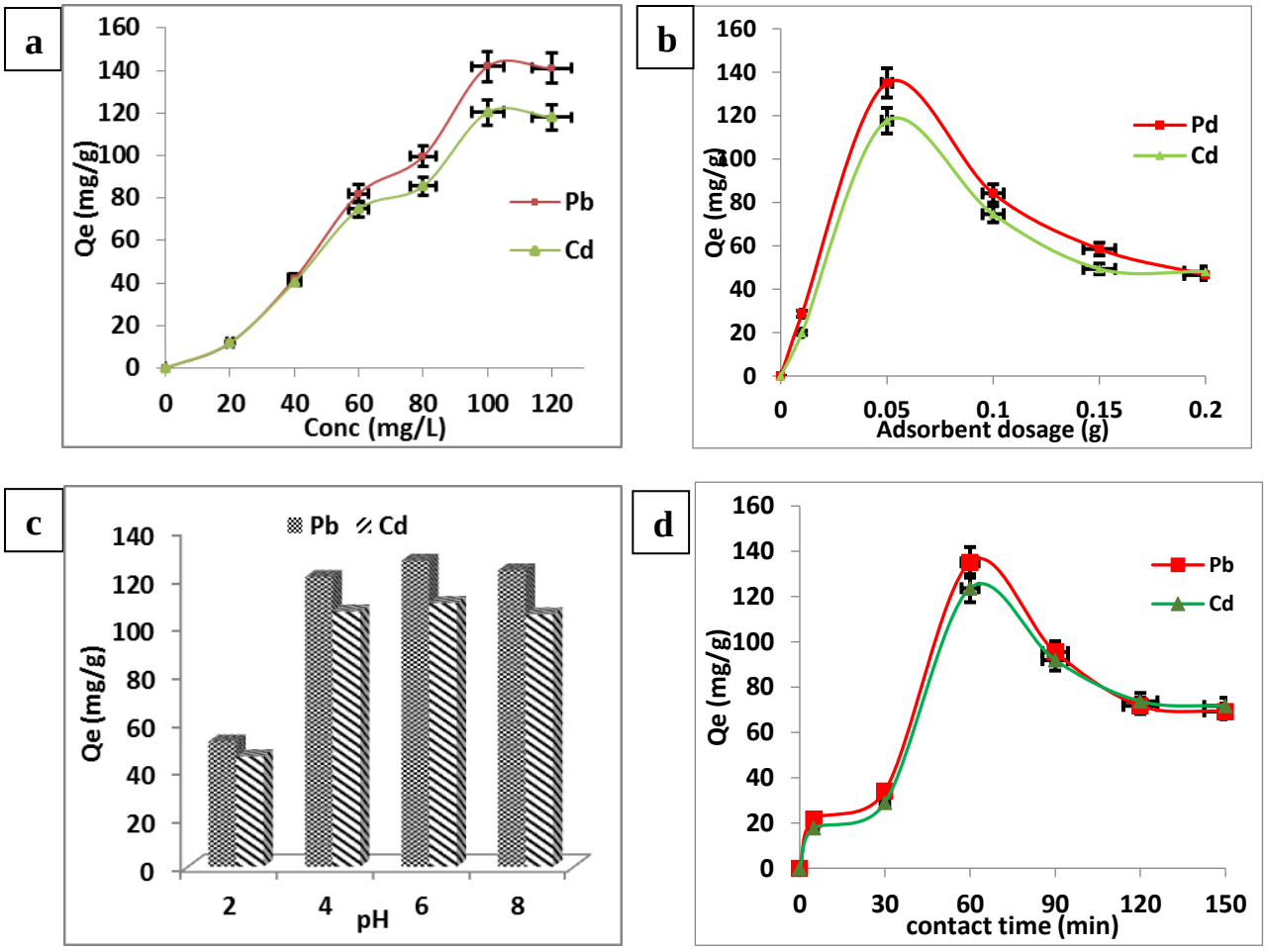

Fig. 6: (a) Effect of initial metal concentration (dose = 0.05 g, time = 60 min, pH = 6) (b) SKN dosage (conc. = 100 mg/L, time = 60 min, pH = 6) (c) solution pH (conc. = 100 mg/L, dose = 0.05 g, time = 60 min) and (d) denotes contact time (conc = 100 mg/L, dose = 0.05 g, pH = 6).

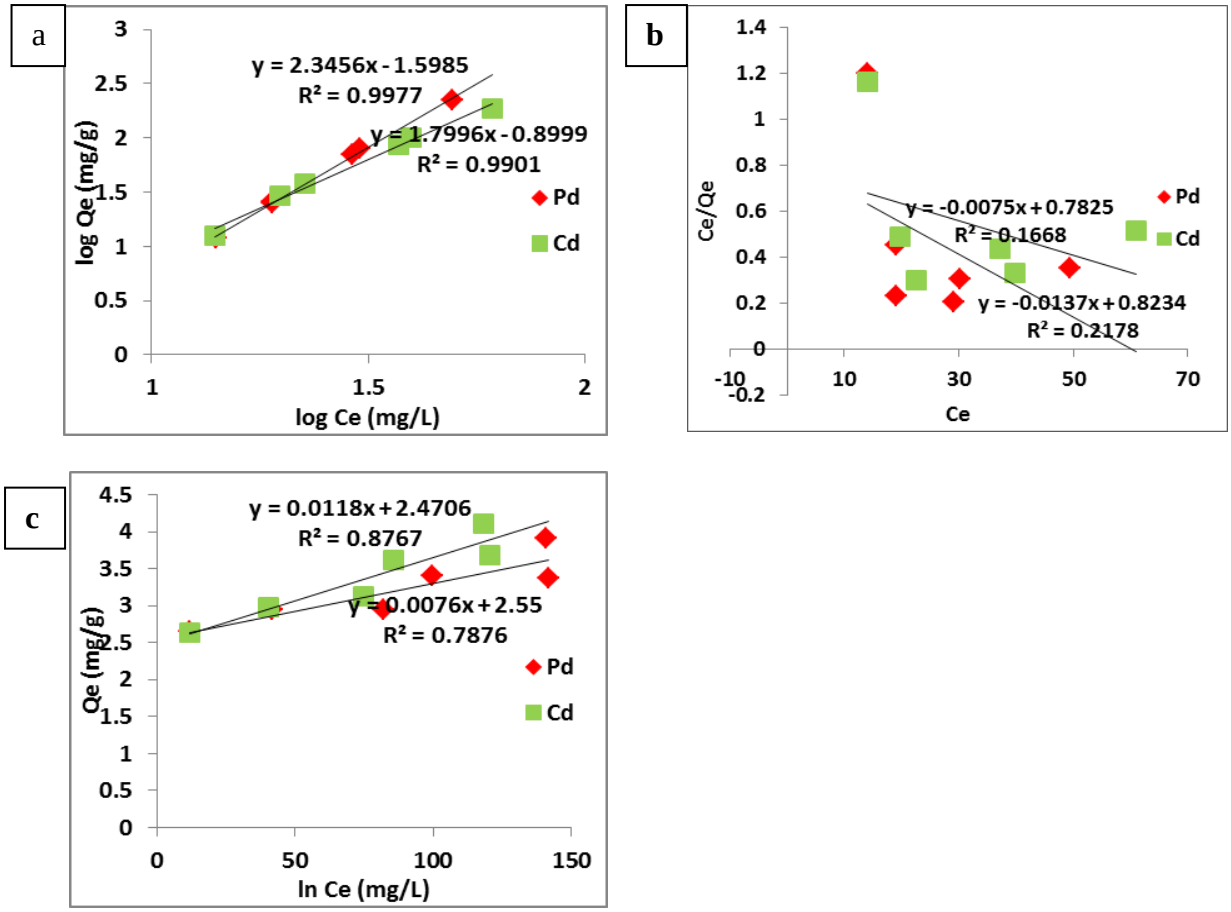

Fig. 7: (a) Freundlich isotherm (b) Langmuir isotherm and (c) Temkin isotherm model

Table 7: Comparison of different adsorbents with Silver-kaolinite nanocomposite (SKN)

Adsorbent	Adsorbate	Maximum quantity adsorbed (mg/g)	References
Biogenic vaterite	Cd^{2+}, Ni^{2+}, and Cu^{2+}	30.30, 94.34 and 175.44	(Liu and Lian, 2019)
Shrimp shell waste	Fe^{2+} and Mn^{2+}	17.43 and 3.87	(Nunez-Gomez *et al.* 2019)
Zinc oxide nanoparticles	Zn^{2+}, Cd^{2+}, and Hg^{2+}	357, 387 and 714	(Sheela *et al.* 2012)
Polyphosphate-modified kaolin	Pb^{2+}, Zn^{2+} and Cd^{2+}	40, 27.78 and 13.23	(Amer *et al.* 2010)
Silver-kaolinite nanocomposite (SKN)	Pb^{2+} and Cd^{2+}	142 and 120	This study

Declarations

Authors contribution

Conceptualization: Solomon, E. Shaibu, Edu J. Inam and Eno A. Moses; Methodology: Solomon, E. Shaibu, Edu J. Inam and Eno A. Moses; Formal analysis and investigation: Solomon, E. Shaibu; Writing - original draft preparation: Solomon, E. Shaibu; Writing - review and editing: Solomon, E. Shaibu, Edu J. Inam and Eno A. Moses; Funding acquisition: Eno A. Moses; Resources: Solomon, E. Shaibu, Edu J. Inam and Eno A. Moses; Supervision: Edu J. Inam and Eno A. Moses.

Conflict of interests

The authors have no known conflict of interest to declare.

Acknowledgements

The authors appreciate the contributions of Ubong J. Etim and Fapojuwo P. Dele for their assistance in the characterizations of the nanocomposites and technical advice.

Funding

This work was supported by Tertiary Education Trust Fund (TETFund) years 2016 – 2018 (merged) TETFund Research Projects (TRP) Intervention.

Availability of data and materials

The authors confirm that the data supporting the findings of this study are available within the article and its supplementary materials.

References

Acevedo, F. J., Jiménez, J., Maldonado, S., Domínguez, E. & Narváez, A. (2007). Classification of wines produced in specific regions by UV− visible spectroscopy combined with support vector machines. *Journal of Agricultural and Food Chemistry*, 55(17): 6842-6849.

Adesuyi, A. O. Awosanya, O. A. Adaramola, F. B. & Omeonu, A. I. (2012). Nutritional and Phytochemical Screening of *Aloe barbadensis*. *Current Research of Journal Biological Science*, 4(1): 4-9.

Alshameri, A., He, H., Zhu, J., Xi, Y., Zhu, R., Ma, L. & Tao, Q. (2018). Adsorption of ammonium by different natural clay minerals: characterization, kinetics and adsorption isotherms. *Applied Clay Science*, 159: 83-93.

Amer, M. W., Khalili, F. I. & Awwad, A. M. (2010). Adsorption of lead, zinc and cadmium ions on polyphosphate-modified kaolinite clay. *Journal Of Environmental Chemistry and Ecotoxicology* (2(1): 001-008.

Arthur, J. D., Langhus, B. G. & Patel, C. (2005). Technical summary of oil gas produced water treatment technologies. *All Consulting, LLC, Tulsa OK*.

Assi, M. A., Hezmee, M. N. M., Haron, A. W., Sabri, M. Y. M. & Rajion, M. A. (2016). The detrimental effects of lead on human and animal health. *Veterinary World*, 9(6): 660.

Aziz, S. G. G., Pashaiasl, M., Khodadadi, K. Ocheje, O. (2019). Application of nanomaterials in three-dimensional stem cell culture. *Journal of Cellular Biochemistry*, 120 (11): 1-9.

Balachandar, R., Gurumoorthy, P., Karmegam, N., Barabadi, H., Subbaiya, R., Anand, K. & Saravanan, M. (2019). Plant-mediated synthesis, characterization and bactericidal potential of emerging silver nanoparticles using stem extract of Phyllanthuspinnatus: a recent advance in phytonanotechnology. *Journal of Cluster Science*, 30(6): 1481-1488.

Barbieri, M., Sappa, G. & Nigro, A. (2018). Soil pollution: Anthropogenic versus geogenic contributions over large areas of the Lazio region. *Journal of Geochemical Exploration*, 195: 78-86.

Battaglia, S., Leoni, L., & Sartori, F. (2006). A method for determining the CEC and chemical composition of clays via XRF. *Clay Minerals*, 41(3), 717-725

Benzidia, B., Barbouchi, M., Hammouch, H., Belahbib, N., Zouarhi, M., Erramli, H. & Hajjaji, N. (2019). Chemical composition and antioxidant activity of tannins extract from green rind of Aloe vera (L.) Burm. F. *Journal of King Saud University-Science*, 31(4): 1175-1181.

Bhowmick, S., Chakraborty, S., Mondal, P., Van Renterghem, W., Van den Berghe, S., Roman-Ross, G. Iglesias, M. (2014. Montmorillonite-supported nanoscale zero-valent iron for removal of arsenic from aqueous solution: Kinetics and mechanism. *Chemical Engineering Journal,* 243: 14-23.

Botes, L., Van der Westhuizen, F. H. & Loots, D. T. (2008). Phytochemical contents and antioxidant capacities of two Aloe greatheadii var. davyana extracts. *Molecules*, 13(9): 2169-2180.

Bourliva, A., Michailidis, K., Sikalidis, C., Filippidis, A. & Betsiou, M. (2013). Lead removal from aqueous solutions by natural Greek bentonites. *Clay Minerals*, 48(5): 771-787.

Cheng, Y., Xing, J., Bu, C., ZHAN, J., Piao, G., Huang, Y., Xie, H. & Wang, X. (2019). Dehydroxylation and structural distortion of kaolinite as high-temperature sorbent in the furnace. *Minerals*, 9(10): 587.

Clay, L. & Pichtel, J. (2019). Treatment of Simulated Oil and Gas Produced Water via Pilot-Scale Rhizofiltration and Constructed Wetlands. *International Journal of Environmental Research,* 13(1): 185- 198.

Dahlan, A. S. (2019). Smart and Functional Materials Based Nanomaterials in Construction Styles in Nano-Architecture. *Silicon*, 11(4): 1949-1953.

de Freitas, F., Battirola, L. D., Arruda, R. & de Andrade, R. L. T. (2019). Assessment of the Cu (II) and Pb (II) removal efficiency of aqueous solutions by the dry biomass Aguapé: kinetics of adsorption. *Environmental Monitoring and Assessment*, 191(12): 751.

Deng, F., Luo, X. B., Ding, L. & Luo, S. L. (2019). Application of nanomaterials and nanotechnology in the reutilization of metal ion from wastewater, In: X. Luo, F. Deng (Editors), *Nanomaterials for the Removal of Pollutants and Resource Reutilization*. Elsevier, pp. 149-178.

Dorathi, P. J. & Kandasamy, P. (2012). Dechlorination of chlorophenols by zero valent iron impregnated silica. *Journal of Environmental Sciences,* 24(4): 765-773.

Errais, E., Duplay, J., Elhabiri, M., Khodja, M., Ocampo, R., Baltenweck-Guyot, R., & Darragi, F. (2012). Anionic RR120 dye adsorption onto raw clay: Surface properties and adsorption mechanism. *Colloids and Surfaces A: Physicochemical and Engineering Aspects*, 403, 69-78.

Eren, Z. & Acar, F. N., (2006). Adsorption of Reactive Black 5 from an aqueous solution: equilibrium and kinetic studies. *Desalination*, 194: 1-10.

Fakhru'l-Razi, A., Pendashteh, A., Abdullah, L. C., Biak, D. R. A., Madaeni, S. S. & Abidin, Z. Z. (2009). Review of technologies for oil and gas produced water treatment. *Journal of Hazardous Materials*, 170(2-3): 530-551.

Fan, W., Liberati, B., Novak, M., Cooper, M., Kruse, N., Young, D. & Trembly, J. (2016). Radium-226 Removal from Simulated Produced Water Using Natural Zeolite and Ion-Exchange Resin. *Industrial Engineering Chemistry Research,* 55(48): 12502–12505.

Foo, K. Y. & Hameed, B.H. (2010). Insights into the modeling of adsorption isotherm systems. *Chemical Engineering Journal*, 156: 2–10.

Freitas, F., Battirola, L. D. & Andrade, R. L. T. (2018b). Adsorption of Cu^{2+} and Pb^{2+} ions by Pontederiarotundifolia (L.f.) (Pontederiaceae) and Salvinia biloba Raddi (Salviniaceae) biomass. *Water, Air, Soil Pollution,* 229: 2–12.

Gao, L., Wang, Z., Li, S. & Chen, J. (2018). Bioavailability and toxicity of trace metals (Cd, Cr, Cu, Ni, and Zn) in sediment cores from the Shima River, South China. *Chemosphere*, 192: 31-42.

Gao, W., Zhao, S., Wu, H., Deligeer, W. & Asuha, S. (2016). Direct acid activation of kaolinite and its effects on the adsorption of methylene blue. *Applied Clay Science*, 126: 98-106.

Ghosh, D. & Bhattacharyya, K. G. (2002). Adsorption of methylene blue on kaolinite. *Applied Clay Science (*20(6): 295–300.

Gupta, S. S. & Bhattacharyya, K. G. (2008). Immobilization of Pb(II), Cd(II) and Ni(II) ions on kaolinite and montmorillonite surfaces from aqueous medium. *Journal of Environmental Management*, 87:46–58

Hao, Z., Chen, L., Wang, C., Zou, X., Zheng, F., Feng, W. & Peng, L. (2019). Heavy metal distribution and bioaccumulation ability in marine organisms from coastal regions of Hainan and Zhoushan, China. *Chemosphere*, 226: 340-350.

Henglein, A., (1998). Colloidal silver nanoparticles: photochemical preparation and interaction with O_2, CCl_4, and some metal ions. *Chemistry of Materials*, 10(1): 444-450.

How, H. K. & Yaacob, W. Z. W. (2015). Synthesis and characterization of marine clay-supported nano zero valent iron. *American Journal of Environmental Sciences*, 11(2): 115.

Hu, Q. H., Qiao, S. Z., Haghseresht, F., Wilson, M. A. & Lu, G. Q. (2006). Adsorption study for removal of basic red dye using bentonite. *Industrial Engineering Chemistry Research*, 45(2): 733-738.

Jiang, M., Jin, X., Lu, X. & Chen, Z. (2010). Adsorption of Pb(II), Cd(II), Ni(II) and Cu(II) onto natural kaolinite clay. *Desalination*, 252:33–39.

Khan, M.R., Rizvi, T.F. & Ahamad, F. (2019). Application of Nanomaterials in Plant Disease Diagnosis and Management. In: K. Abd-Elsalam, R. Prasad (Editors), *Nanobiotechnology Applications in Plant Protection. Nanotechnology in the Life Sciences*. Springer, Cham, pp. 19-33. https://doi.org/10.1007/978-3-030-13296-5_2..

Kim, S. A., Kamala-Kannan, S., Lee, K. J., Park Y. J., Shea, P. J., Lee, W. H., Kim, H. M. & Oh, B. T. (2013). Removal of Pb(II) from aqueous solution by a zeolite–nanoscale zero-valent iron composite. *Chemical Engineering Journal*, 217: 54-60.

Kouassi, N., Yao, K. M., Sangare, N., Trokourey, A. & Metongo, B. S. (2019). Correction to: The mobility of the trace metals copper, zinc, lead, cobalt, and nickel in tropical estuarine sediments, Ebrie Lagoon, Côte d'Ivoire. *Journal of Soils and Sediments*, 19(2): 929-944.

Koyuncu, H., Kul, A. R., Yıldız, N., Çalimli, A. & Ceylan, H. (2007). Equilibrium and kinetic studies for the sorption of 3-methoxybenzaldehyde on activated kaolinites. *Journal of Hazardous Materials*, 141(1): 128-139.

Kumar, S. (2006). Spectroscopy of organic compounds. *Cosmic Rays*, 10: 4.

Kumric, K. R, Đuckic, A. B, Trtic´-Petrovic, T. M., Vukelic, N. S., Stojanovic, Z., Grbovic, N. & Matovic, L. L. (2013). Simultaneous removal of divalent heavy metals from aqueous solutions using raw and mechanochemically treated interstratified montmorillonite/kaolinite clay. *Industrial Engineering Chemistry Research*, 52: 7930–7939.

Li, C., Huang, Y., Dong, X., Sun, Z., Duan, X., Ren, B. & Dionysiou, D. D. (2019). Highly efficient activation of peroxymonosulfate by natural negatively-charged kaolinite with abundant hydroxyl groups for the degradation of atrazine. *Applied Catalysis B: Environmental,* 247: 10-23.

Liao, P., Yuan, S., Xie, W., Zhang, W., Tong, M., Wang, K. (2013. Adsorption of nitrogen-heterocyclic compounds on bamboo charcoal: kinetics, thermodynamics, and microwave regeneration. *Journal of Colloid and Interface Science*, 390(1): 189-195.

Lin, Y. H., Tseng, H. H., Wey, M. Y. & Lin, M. D. (2010). Characteristics of two types of stabilized nano zero-valent iron and transport in porous media. *Science of the Total Environment*, 408(10): 2260-2267.

Liu, R. & Lian, B. (2019). Non-competitive and competitive adsorption of Cd^{2+}, Ni^{2+}, and Cu^{2+} by biogenic vaterite. *Science of the Total Environment*, 659: 122–130.

Liu, T., Wang, Z. L., Yan, X. & Zhang, B. (2014). Removal of mercury (II) and chromium (VI) from wastewater using a new and effective composite: Pumice-supported nanoscale zero-valent iron. *Chemical Engineering Journal,* 245: 34-40.

Ma, C. & Eggleton, R. A. (1999). Cation exchange capacity of kaolinite. *Clays and Clay Minerals*, 47(2): 174-180.

Medda, S. Hajra, A., Dey, U., Bose, P. & Mondal, N. K. (2015). Biosynthesis of silver nanoparticles from Aloe vera leaf extract and antifungal activity against Rhizopus sp. And Aspergillus sp. *Applied Nanoscience*, 5(7): 875-880.

Nadagouda, M. N. & Varma, R. S. (2008). Green synthesis of silver and palladium nanoparticles at room temperature using coffee and tea extract. *Green Chemistry*, 10(8): 859-862.

Narayanan, K. B. & Sakthivel, N. (2008). Coriander leaf mediated biosynthesis of gold nanoparticles. *Materials Letters*, 62(30): 4588-4590.

Neff, J., Lee, K. & DeBlois, E.M. (2011). Produced Water: Overview of Composition, Fates, and Effects. In: K. Lee, J. Neff (Editors), *Produced Water*. Springer, New York, pp. 3-54. https://doi.org/10.1007/978-1-4614-0046-2_1.

Nunez-Gomez, D., Rodrigues, C., Lapolli, F. R. & Lobo-Recio, M. A. (2019). Adsorption of heavy metals from coal acid mine drainage by shrimp shell waste: Isotherm and continuous-flow studies. *Journal of Environmental Chemical Engineering*, 7(1): 102787.

Obianwu, V. I., George, N. J. & Okiwelu, A. A. (2011). Preliminary Geophysical Deduction of Lithological and Hydrological Conditions of the North-Eastern Sector of Akwa Ibom State, Southern Nigeria. *Research Journal of Applied Sciences, Engineering and Technology*, *3*(8), 806-811.

O'Carroll, D., Sleep, B., Krol, M., Boparai, H. & Kocur, C. (2013). Nanoscale zero valent iron and bimetallic particles for contaminated site remediation. *Advances in Water Resources*, 51: 104-122.

Ondrasek, G., Rengel, Z. & Romic, D. (2018). Humic acids decrease uptake and distribution of trace metals, but not the growth of radish exposed to cadmium toxicity. *Ecotoxicology and Environmental Safety*, 151: 55-61.

Ouyang, D., Zhuo, Y., Hu, L., Zeng, Q., Hu, Y. & He, Z. (2019). Research on the adsorption behavior of heavy metal ions by porous material prepared with silicate tailings. *Minerals*, 9(5): 291.

Özsin, G., Kılıç, M., Apaydın-Varol, E. & Pütün, A. E. (2019). Chemically activated carbon production from agricultural waste of chickpea and its application for heavy metal adsorption: equilibrium, kinetic, and thermodynamic studies. *Applied Water Science*, *9*(3): 1-14.

Pacheco-Torgal, F. (2019). Introduction to nanotechnology in eco-efficient construction. In: F. Pacheco-Torgal *et al.* (Editors), *Nanotechnology in Eco-efficient Construction*, Elsevier, pp. 1-9. https://doi.org/10.1016/B978-0-08-102641-0.00001-3.

Panda, A. K., Mishra, B. G., Mishra, D. K. & Singh, R. K. (2010). Effect of sulphuric acid treatment on the physico-chemical characteristics of kaolin clay. *Colloids and Surfaces A: Physicochemical and Engineering Aspects*, 363(1-3): 98-104.

Phanjom, P., Sultana, A., Sarma, H., Ramchiary, J., Goswami, K. & Baishya, P. (2012). Plant-mediated synthesis of silver nanoparticles using Elaeagnuslatifolia leaf extract. *Digest Journal of Nanomaterials and Biostructures*, *7*(3): 1117-1123.

Phenrat, T., Saleh, N., Sirk, K., Tilton, R. D. & Lowry, G. V. (2007). Aggregation and sedimentation of aqueous nanoscale zerovalent iron dispersions. *Environmental Science & Technology*, *41*(1): 284-290.

Rauwel, P., Küünal, S., Ferdov, S. & Rauwel, E. (2015). A review on the green synthesis of silver nanoparticles and their morphologies studied via TEM. *Advances in Materials Science and Engineering*, Article ID: 682749. https://doi.org/10.1155/2015/682749.

Reynolds, T. & Dweck, A. C. (1999). Aloe vera leaf gel: A review update. *Journal of Ethnopharmacology,* 68(1-3): 3-37.

Roseline, T. A., Murugan, M., Sudhakar, M. P. & Arunkumar, K. (2019). Nanopesticidal potential of silver nanocomposites synthesized from the aqueous extracts of red seaweeds. *Environmental Technology & Innovation*, 13: 82-93.

Sadasivam, S. & Rao, S. M. (2016). Characterization of silver–kaolinite (AgK): an adsorbent for long-lived 129I species. *SpringerPlus* 5: 142.

Saccù, D., Bogoni, P. & Procida, G. (2001). Aloe exudate: characterization by reversed phase HPLC and headspace GC-MS. *Journal of Agricultural and Food Chemistry*, 49(10): 4526-4530.

Salleh, M. A. M., Sulaiman, O., Mahmoud, D. K., Karim, W. A. W. A. & Idris, A. (2011). Cationic and anionic dye adsorption by agricultural solid wastes: A comprehensive review. *Desalination.* 280: 1-13.

Salman, J. M., Njoku, V. O. & Hameed, B. H. (2011) Adsorption of pesticides from aqueous solution onto banana stalk activated Carbon. *Chemical Engineering Journal,*174: 41– 48

Sánchez-Machado, D. I., López-Cervantes, J., Sendón, R. & Sanches-Silva, A. (2017). Aloe vera: ancient knowledge with new frontiers. *Trends in Food Science & Technology*, 61: 94-102.

Sarkar, B., Rusmin, R., Ugochukwu, U. C., Mukhopadhyay, R. & Manjaiah, K. M. (2019). Modified clay minerals for environmental applications. In: M. Mercurio, B. Sarkar, A. Langella (Editors), *Modified Clay and Zeolite Nanocomposite Materials*. Elsevier, pp. 113-127. https://doi.org/10.1016/B978-0-12-814617-0.00003-7.

Sarma, G. K., Gupta, S. S. & Bhattacharyya, K. G. (2019). Removal of hazardous basic dyes from aqueous solution by adsorption onto kaolinite and acid-treated kaolinite: kinetics, isotherm and mechanistic study. *SN Applied Sciences*, 1(3): 211.

Shankar, S. S., Rai, A., Ahmad, A. & Sastry, M. (2004). Rapid synthesis of Au, Ag, and bimetallic Au core Ag shell nanoparticles using Neem (*Azadirachta indica*) leaf broth. *Journal of Colloid Interface Science, 2*75: 496–502

Sharma, M., Singh, J., Hazra, S. & Basu, S. (2019). Adsorption of heavy metal ions by mesoporous ZnO and TiO_2@ZnO monoliths: Adsorption and kinetic studies. *Microchemical Journal,* 145*:* 105–112.

Sheela, T., Nayaka, Y. A., Viswanatha, R., Basavanna, S. & Venkatesha, T. G. (2012). Kinetics and thermodynamics studies on the adsorption of Zn (II), Cd (II) and Hg (II) from aqueous solution using zinc oxide nanoparticles. *Powder Technology,* 217: 163-170.

Shin, K. H., Woo, W. S., Lim, S. S., Shim, C. S., Chung, H. S., Kennelly, E. J. & Kinghorn, A. D. (1997). Elgonica-dimers A and B, two potent alcohol metabolism inhibitory constituents of Aloe arborescens. *Journal of Natural Products*, 60(11): 1180-1182.

Shukla, A., Zhang, Y. H., Dubey, P., Margrave, J. L. & Shukla, S. S. (2002). The role of sawdust in the removal of unwanted materials from water. *Journal of Hazardous Materials*, 95(1-2): 137-152.

Song, J. Y. & Kim, B. S. (2009). Rapid biological synthesis of silver nanoparticles using plant leaf extracts. *Bioprocess and Biosystems Engineering*, 32(1): 79.

Srinivasan, R. (2011). Advances in application of natural clay and its composites in removal of biological, organic, and inorganic contaminants from drinking water. *Advances in Materials Science and Engineering,* Article ID 872531. https://doi.org/10.1155/2011/872531.

Teow, Y. H. & Mohammad, A. W. (2019). New generation nanomaterials for water desalination: A review. *Desalination*, 451: 2-17.

Torres-Luna, J. A. & Carriazo, J. G. (2019). Porous aluminosilicic solids obtained by thermal-acid modification of a commercial kaolinite-type natural clay. *Solid State Sciences*, 88: 29-35.

Trabelsi, F., Khlifi, R., Goux, D., Guillamin, M., Hamza-Chaffai, A. & Sichel, F. (2016). Genotoxic effects of cadmium in human head and neck cell line SQ20B. *Environmental Science and Pollution Research* (2*3*(16): 16127-16136.

Tran, V. S., Ngo, H. H., Guo, W., Zhang, J., Liang, S., Ton-That, C. & Zhang, X. (2015). Typical low cost biosorbents for adsorptive removal of specific organic pollutants from water. *Bioresource Technology,* 182: 353–363.

Uğurlu, M. & Karaoğlu, M. H. (2011). Adsorption of ammonium from an aqueous solution by fly ash and sepiolite: isotherm, kinetic and thermodynamic analysis. *Microporous and Mesoporous Materials*, *139*(1-3): 173-178.

Umano, K., Nakahara, K., Shoji, A. & Shibamoto, T. (1999). Aroma chemicals isolated and identified from leaves of Aloe arborescens Mill. var. natalensis Berger. *Journal of Agricultural and Food chemistry*, *47*(9): 3702-3705.

Veil, J. A., Puder, M. G., Elcock, D. & Redweik, R. J. (2004). *A White Paper Describing Produced Water from Production of Crude Oil., Natural Gas, and Coal Bed Methane*. U.S. Department of Energy National Energy Technology Laboratoryp.87. Accessed on April 8, 2022 from https://publications.anl.gov/anlpubs/2004/02/49109.pdf.

Vijayaraghavan, K., Padmesh, T. V. N., Palanivelu, K. & Velan, M. (2006). Biosorption of nickel (II) ions onto Sargassum wightii: application of two-parameter and three-parameter isotherm models. *Journal of Hazardous Materials*, *133*: 304-308.

Vikrant, K. & Kim, K. H. (2019). Nanomaterials for the adsorptive treatment of Hg (II) ions from water. *Chemical Engineering Journal*, 358: 264-282.

Wang, H. & Luo, P. (2020). Preparation, kinetics, and adsorption mechanism study of microcrystalline cellulose-modified bone char as an efficient Pb (II) adsorbent. *Water, Air, Soil Pollution*, 2*31*(7): 1-15.

Wani, I. A., Ganguly, A., Ahmed, J. & Ahmad, T. (2011). Silver nanoparticles: ultrasonic wave assisted synthesis, optical characterization and surface area studies. *Materials Letters*, *65*(3): 520-522.

Wintola, O. A. & Afolayan, A. J. (2011). Phytochemical constituents and antioxidant activities of the whole leaf extract of Aloe ferox Mill. *Pharmacognosy Magazine*, *7*(28): 325.

Yuan, P., Fan, M., Yang, D., He, H., Liu, D., Yuan, A. & Chen, T. (2009). Montmorillonite-supported magnetite nanoparticles for the removal of hexavalent chromium [Cr (VI)] from aqueous solutions. *Journal of Hazardous Materials*, 166: 821-829.

Zhu, W., Chen, Z., Pan, Y., Dai, R., Wu, Y., Zhuang, Z. & Li, Y. (2019). Functionalization of hollow nanomaterials for catalytic applications: Nanoreactor construction. *Advanced Materials*, *31*(38): 1800426.